COMPARATIVE EFFICIENCY OF FINITE ELEMENT MODELS OF CFRP BONDED JOINTS

J. Díaz, L. Romera, S. Hernández, A. Baldomir
Structural Engineering Department, University of La Coruña

Keywords: *Adhesive bonded joint, single-lap joint, nonlinear finite element analysis.*

Abstract

Bonded joints are a common system of connection in aeronautical and space structures. By using adhesive materials, many structural parts made of carbon fiber reinforced plastic (CFRP) can be effectively linked. A specific issue in this type of joints is constituted by the evaluation of the stress and strain fields in the adhesive material. Obviously, experimental works can be carried out in laboratory in order to identify the ultimate load value, but numerical methods based on finite element structural models can be very useful in describing the stress and strain response for each load step.

In this approach, an issue regarding to the accuracy of the several finite element discretizations used to describe the joint is under debate. In this paper a parametric study aimed to compare the accuracy of several modelizations of a bonded joint consisting of two parts of CFRP bonded by a layer of epoxy film adhesive will be presented. All the finite elements models developed are three-dimensional and they include the geometrical nonlinearity of the single lap behaviour with linear elastic materials in the adherend and the adhesive. Results obtained with different mesh sizes and element types are compared with the available experimental data. Finally in one model the effect of material nonlinearity in the adhesive is analyzed using a traction-separation linear damage model with cohesive elements.

1 Introduction

The study of structural bonded joints started at the first half of the XX Century, with the works of Volkersen [1] and Goland and Reissner [2], revised and extended later by Hart-Smith, who dedicated studies to the general behavior of the single lap joint [3] as well as to the particular case of adherends made of composite material [4].

The first analytic methods were complemented by experimental works focused on the evaluation of the deformational response of the joint and it's strength. Often, these studies were accompanied with finite element models (FEM) validated with the experimental results.

Tsai and Morton [5] developed a three-dimensional FEM of the single lap joint with metallic adherends and carried out a linear static analysis, proving the spatial nature of the deformational response and putting in evidence that the interior stresses in the adhesive layer are quite different from those at the exterior face. This FEM was verificated against their own experimental results, obtained with Moiré interferometry.

After that, the tests were repeated considering adherends made of composite material [6], comparing the response with a bidimensional FEM in plane strain analyzed using non linear theory with geometrical nonlinearity. The results have been verified numerically by Li et al. [7] with a bidimensional mesh of which the behavior throughout the thickness is extracted, not only in the middle plane.

The disadvantage of the previous modeli-

zations is that the 2D meshes cannot capture the effect of in-plane shear and bending-twisting coupling caused by the fiber layers with orientations of $\pm 45°$. This is the reason why the present job has been developed, where the main objetive is the parametric comparative study of the precision of the stress and strain response in the adhesive layer of a single lap bonded joint with composite adherends, taking into account diferent element types, mesh discretizations and analysis procedures in a tridimensional mesh. The purpose is to deduce the better metodology to include this kind of joints in global models, in order to get the combined response.

2 The Single-lap Joint Finite Element Model

The analysis of the three-dimensional behavior of the single lap bonded joint was performed with a model of the same dimensions as the one used by Tsai and Morton [6], so that the results obtained could be verified with the experimental data obtained by these authors. The Fig. 1 shows the geometrical definiton and also the origin and orientation of the global coordinate system, along with the boundary conditions applied at the adherents ends. The dimension values are shown in Table 1.

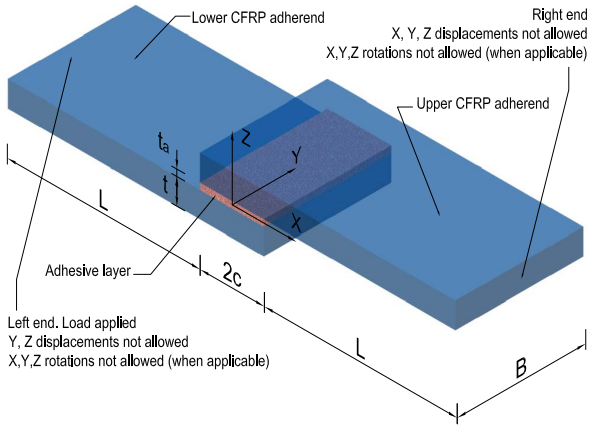

Fig. 1 Geometrical definiton of the CFRP single lap joint

The material of the adherends is graphite/epoxy (XAS/914C) with a lay-up of $[0/45/-45/0]_{2c}$ and the adhesive layer is made of epoxy resin HEXCEL Redux 308A. The properties of each material are showed Table 2, where the hypothesis made for each ortotrophic lamina are $E_z = E_y$, $G_{xy} = G_{xz} = G_{yz}$ and $\nu_{xy} = \nu_{xz} = \nu_{yz}$.

L (mm)	$2c$ (mm)	t (mm)	t_a (mm)	B (mm)
101.6	25.4	2.0	0.13	25.4

Table 1 Dimensions of the model

The applied load is 4448 N at the end cross section surface of the lower CFRP adherend (Fig. 1). The boundary conditions at the loaded adherend end restrict all the degrees of freedom (DOF), except for the longitudinal displacement, while at the unloaded adherend end, none of the displacements or rotations are allowed when the element type has this DOF in its formulation.

Symmetry conditions have also been applied in the middle longitudinal plane of the joint, at $Y = B/2$. That is the reason why the width of the mesh is reduced to half, imposing the conditions of null cross-sectional displacement in the symmetry plane.

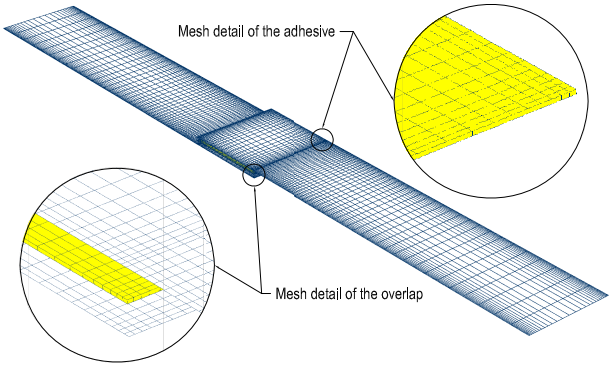

Fig. 2 Finite element model of the joint and details of the mesh refinement at the overlap end with shell adherends and cohesive elements at the adhesive layer

The analysis code used was ABAQUS/Standard in its version 6.5-5 [8], considering two different element types for the adherent as well as for the adhesive, with the purpose of verifying its behavior for a possible inclusion in a global model.

Material	E_x (GPa)	E_y (GPa)	G_{xy} (GPa)	ν_{xy}
Composite lamina	138	9.4	6.7	0.32
Epoxy adhesive	3	3	1.15	0.31

Table 2 Material properties of adherend and adhesive

At the adherends four node shell elements with full integration have been used with six DOF per node without hourglass modes neither in membrane nor in bending response [9]. In order to connect these elements with those of the adhesive layer, kinematic couplings have been applied considering the rotation and the displacement of the nodes of the interface between adherend and adhesive. Also hexaedrical elements of eight nodes, called "continuum shell" in the program, were employed in the adherend . These elements present a volumetric connectivity and have three DOF at each node, but their kinematic and constitutive behavior is similar to conventional shell elements.

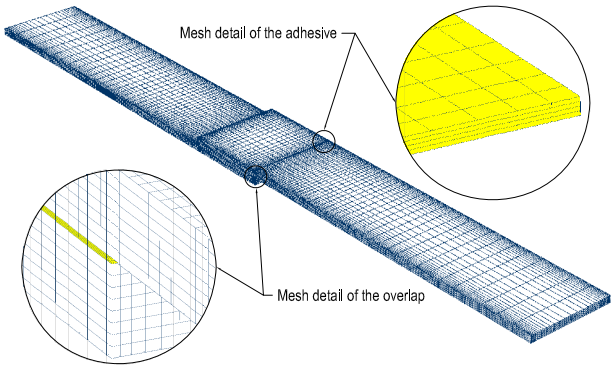

Fig. 3 Finite element model of the joint and details of the mesh refinement at the overlap end with continuum shell adherends and solid elements for the adhesive layer

With respect to the adhesive, we used in most of the cases a two layer discretization with eight nodes solid elements and three DOF per node with reduced integration and hourglass control. In addition, a specially formulated element for adhesive layers, called "cohesive" in the program, has been used. It is an hexaedrical element with eight nodes and three DOF per node that can mesh the adhesive with only a layer of elements.

The Fig. 2 shows a FEM of the joint with shell elements for the adherends and cohesive elements for the adhesive layer, whereas in the Fig. 3 continuum shell elements are used at the adherends and solid elements for the adhesive layer

On the other hand, the finite element mesh has been parametrized based on the following variables:

- E_l: Number of elements in longitudinal direction at the non-overlapped section of the adherends.
- E_{la}: Number of elements in the longitudinal direction at the overlap of adherend and adhesive.
- E_v: Number of elements in vertical direction at the adherends.
- E_{va}: Number of elements in vertical direction at the adhesive layer.
- E_t: Number of elements in transversal direction.

Considering the variation of these parameters and the combination of element types, 26 different models have been defined, grouped in 6 categories, according to the Table 3.

The F00 model is considered as the reference to verify the mesh and its discretization which tries to obtain the experimental response measured by Tsai and Morton [6], serving as base to elaborate the rest of models.

The models of groups 1 and 2 are destined to evaluate the influence of the longitudinal (E_{la}) and vertical (E_{va}) discretización respectively in the adhesive layer, whereas groups 3 and 4 pursue the same objective in the adherend (E_l and E_v). Group 5 considers the influence of the element

Group	*Model*	*Number of elements*					*Total*		*Element Type*	
		E_l	E_{la}	E_v	E_{va}	E_t	*Elements*	*Nodes*	*Adherend*	*Adhesive*
0	F00	100	160	1	2	20	16800	21105	Shell	Solid
1	F01	50	20	1	4	20	4400	5187	Shell	Solid
1	F02	50	40	1	4	40	13600	15867	Shell	Solid
1	F03	50	60	1	4	60	27600	32147	Shell	Solid
1	F04	50	80	1	4	80	46400	54027	Shell	Solid
1	F05	50	100	1	4	100	70000	81507	Shell	Solid
2	F06	50	60	1	1	60	16800	20984	Shell	Solid
2	F07	50	60	1	2	60	20400	24705	Shell	Solid
2	F08	50	60	1	4	60	27600	32147	Shell	Solid
2	F09	50	60	1	6	60	34800	39589	Shell	Solid
2	F10	50	60	1	8	60	42000	47031	Shell	Solid
3	F11	10	60	1	4	60	22800	27267	Shell	Solid
3	F12	25	60	1	4	60	17500	20757	Shell	Solid
3	F13	50	60	1	4	60	27600	32147	Shell	Solid
3	F14	100	60	1	4	60	33600	38247	Shell	Solid
3	F15	200	60	1	4	60	45600	50447	Shell	Solid
4	F16	50	60	1	4	60	27100	38247	C. Shell	Solid
4	F17	50	60	2	4	60	40800	51789	C. Shell	Solid
4	F18	50	60	4	4	60	67200	78873	C. Shell	Solid
4	F19	50	60	8	4	60	120000	133041	C. Shell	Solid
4	F20	50	60	16	4	60	225600	241377	C. Shell	Solid
5	F21	50	100	1	2	100	50000	61105	Shell	Solid
5	F22	50	100	4	2	100	140000	162711	C. Shell	Solid
5	F23	50	100	1	1	100	40000	50904	Shell	Cohesive
5	F24	50	100	4	1	100	130000	152510	C. Shell	Cohesive
6	F25	25	20	1	1	10	2200	2814	Shell	Cohesive

Table 3 Characterization of the models involved in the parametric study, including mesh size and type of finite element used

type in the behavior of the union, defining all the possible combinations.

Finally, the F25 model has been used to study the adhesive taking into account nonlinearity of the material by damage. Regarding to the analysis mode, the verification model F00 was analyzed using linear theory as well as nonlinear considering geometrical nonlinearity. It is verified that the analysis with geometrical nonlinearity performs a more precise behavior of the joint. For this reason, the rest of analysis has been always made in nonlinear theory.

3 Results and Discussion

3.1 Verification of the Reference Model

The Fig. 4 shows the peel (σ_z) and shear τ_{xz} strain distribution with both linear and nonlinear analysis in model F00, along with the Tsai and Morton's [6] results in the middle plane of the adhesive layer (Y=0). It is verified that the linear analysis does not represent the shear strains properly, specially in the final third of the curve. Nevertheless, the nonlinear model correctly fits the experimental curve, except in the zone where the pronounced growth begins ($0.55 < x/c < 0.9$).

Accurate results are achieved at the final section, where the strains are around 3.5%, obtaining total coincidence between numerical and experimental data.

With regard to the peeling strain, the difference between models is smaller, although nonlinear one obtains again the better response, displaying disagreement with the tests in the zone of $0,7 < x/c < 0.95$. It is possible to indicate as a positive aspect that the maximum strains, located at the end of adhesive layer are obtained correctly by the model. Normalized analysis time, that compares the computational cost of all the considered models shows a result of 0.017 against 0.009 in favor of the linear model. Fig. 5 shows the deformed shape of the model, with a scale factor of 20.

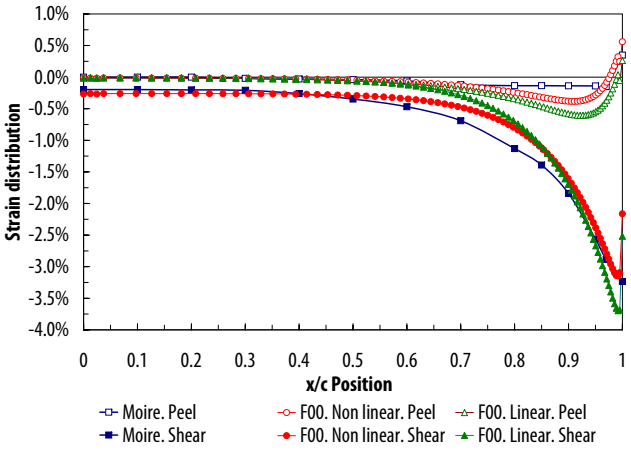

Fig. 4 Comparison of strains measured in Tsai and Morton's Moire experiment [6] and the reference model F00 along the centerline of the adhesive layer for linear and nonlinear analysis

Fig. 5 Deformed shape of the CFRP single lap joint

The Fig. 6 shows the contour plot of the peeling stresses at the middle plane of the adhesive layer, where is clearly seen the stress concentration at the longitudinal and transversal ends of the overlap. The same thing happens with normal stresses σ_x (Fig. 7) and with shear stresses τ_{xz} (Fig. 8), being in this case the transversal variation unimportant.

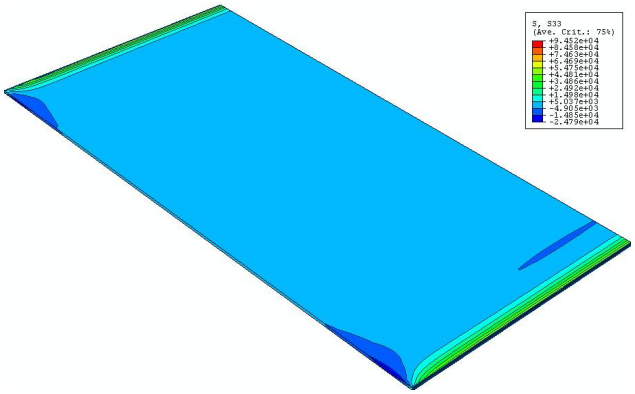

Fig. 6 Contour map of the σ_z peel stresses at the adhesive layer

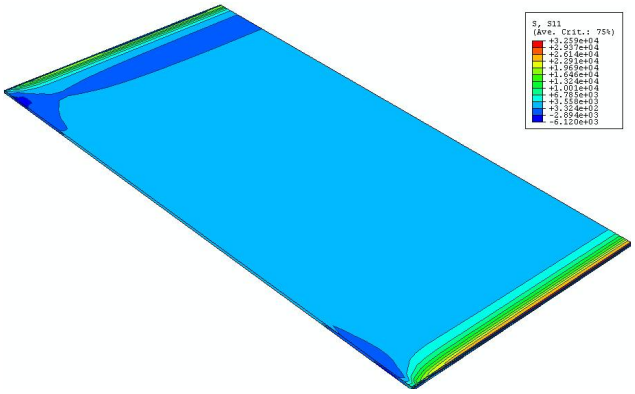

Fig. 7 Contour map of the σ_x stresses at the adhesive layer

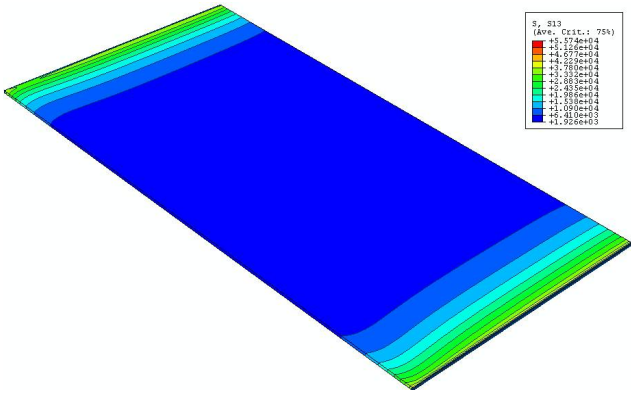

Fig. 8 Contour map of the τ_{xz} shear stresses at the adhesive layer

3.2 Mesh Discretization Influence

All the stress results have been normalized with respect to the average stress p in the adherent, that is equal to 87.56 MPa.

In the models of group 1 the influence of the longitudinal discretization of the adhesive is studied. Fig. 9 shows the distribution of strains, where it is specially observed that this parameter has a significant influence, when considering the peaks of strain at the end of the union. This influence is appreciable also with strain stresses and is very important for obtaining of the peeling stresses, which is shown in the Fig. 10.

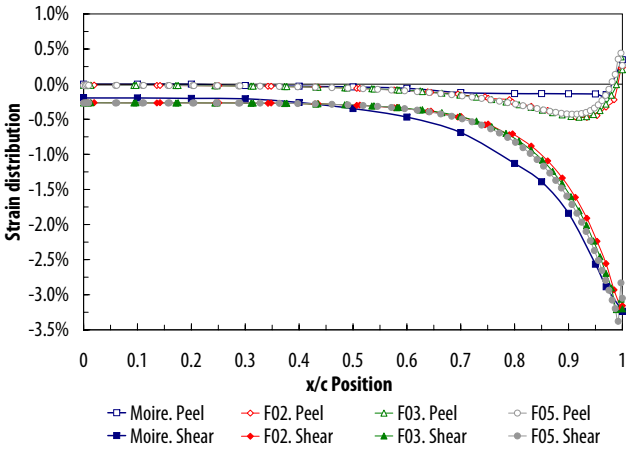

Fig. 9 Comparison of strains measured in Tsai and Morton's Moire experiment [6] and the F02, F03 and F05 models, involving longitudinal discretization influence of the adhesive layer mesh

In group 2 the importance of the vertical discretizaction of the adhesive layer is considered, and it was proved to be practically null for the case of the strains (Fig. 11) and very small in the case of the stresses (Fig. 12). This is logical considering that all the results have been obtained in the middle line of the adhesive. If our intention is to study the structural response throughout the thickness, then finer discretizations will have to be taken into acount, being able to avoid it otherwise.

In the case of the adherends mesh, the longitudinal discretization does not affect to the results (Fig. 13). However in this case since the number of elements considered in this analysis is higher

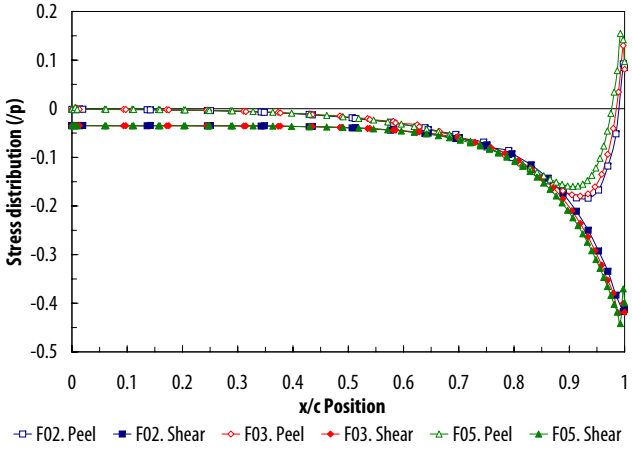

Fig. 10 Stress distribution in F02, F03 and F05 models, involving longitudinal discretization influence of the adhesive layer mesh

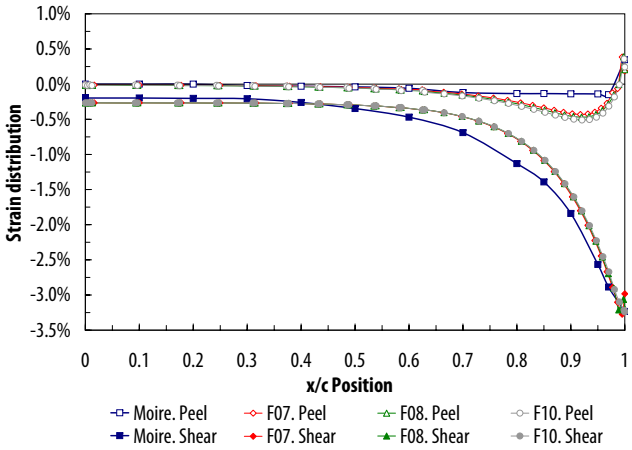

Fig. 11 Comparison of strains measured in Tsai and Morton's Moire experiment [6] and the F07, F08 and F10 models, involving vertical discretization influence of the adhesive layer mesh

in all the cases to the really necessary ones to obtain the structural response. A case of overmeshing can be considered, that it is confirmed by the coincidence of all the results of stress (Fig. 14). In this case it can be considered reasonable to use a coarser discretization.

The number of elements used in the vertical discretization of the adherent when continuum shell elements are employed has a significant influence in the results at the adhesive layer, especially in the case of the stresses, as shown in Fig. 16. In this case, a smaller number of elements presents better results, obtaining a good

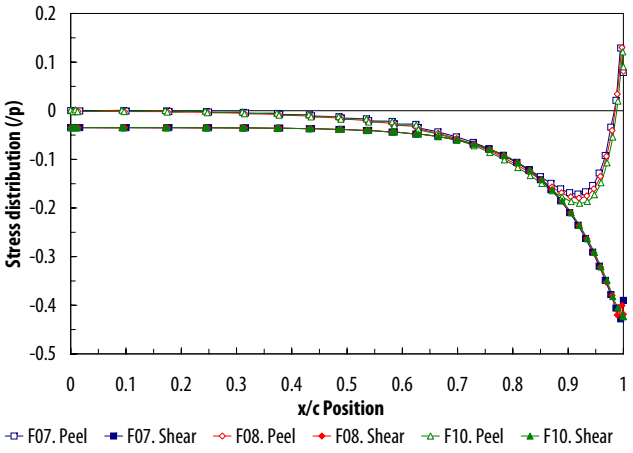

Fig. 12 Stress distribution in F07, F08 and F10 models, involving vertical discretization influence of the adhesive layer mesh

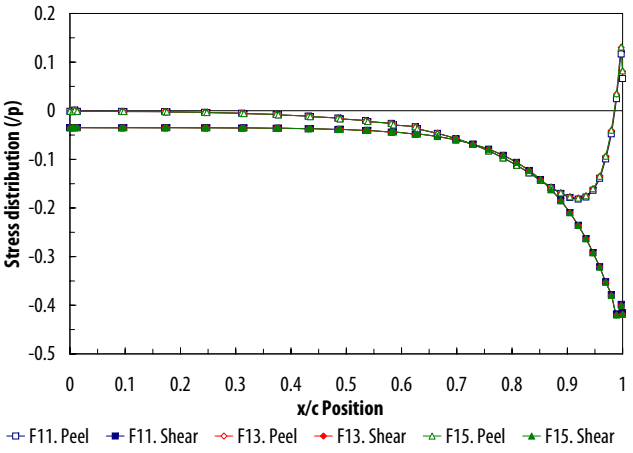

Fig. 14 Stress distribution in F11, F13 and F15 models, involving longitudinal discretization influence of the adherent mesh

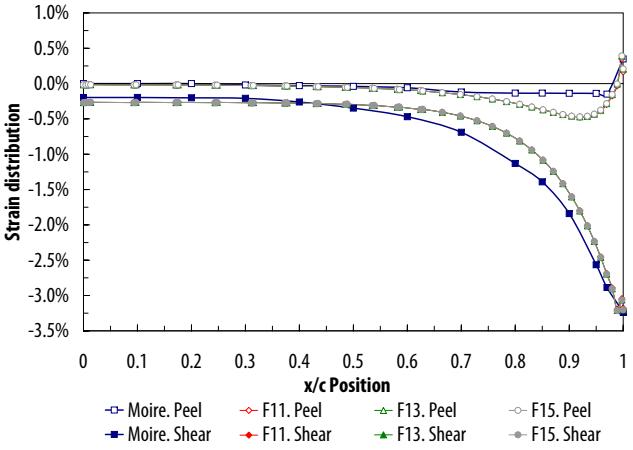

Fig. 13 Comparison of strains measured in Tsai and Morton's Moire experiment [6] and the F11, F13 and F15 models, involving longitudinal discretization influence of the adherent mesh

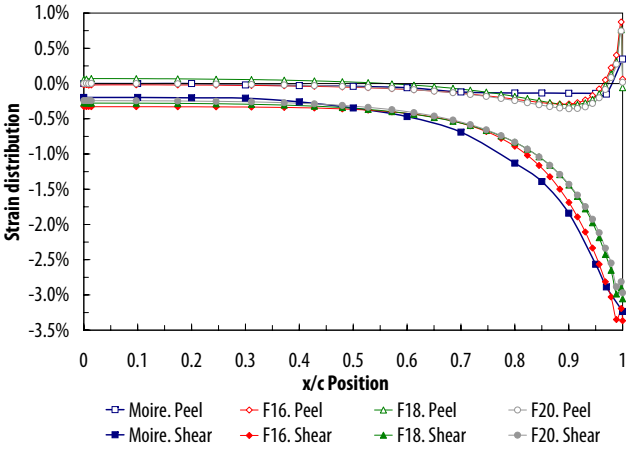

Fig. 15 Comparison of strains measured in Tsai and Morton's Moire experiment [6] and the F16, F18 and F20 models, involving vertical discretization influence of the adherent mesh

adjustment of the strains in the final part of overlap (Fig. 15). This is because when we increase this value, the elements are much more small in vertical direction, taking place a great distortion that penalizes the results.

3.3 Element type influence

When we approximate the shear strain and stresses, the best models are those with shell elements at the adherend (Fig. 17 and Fig. 18). We obtain better results of the model using solid elements in the adhesive, because it uses one more layer of elements, although the cohesive element is specially formulated for these cases. On the other hand, they display greater precision in the peeling stresses and strains in the models that use solids in the adhesive.

3.4 Computational Cost

The Fig. 19 show the normalized analysis time for each model. It is observed that the most expensive models are those that use continuum shell elements when several elements for adherent zones are used. The results obtained in the previous sections, along with the longer calcula-

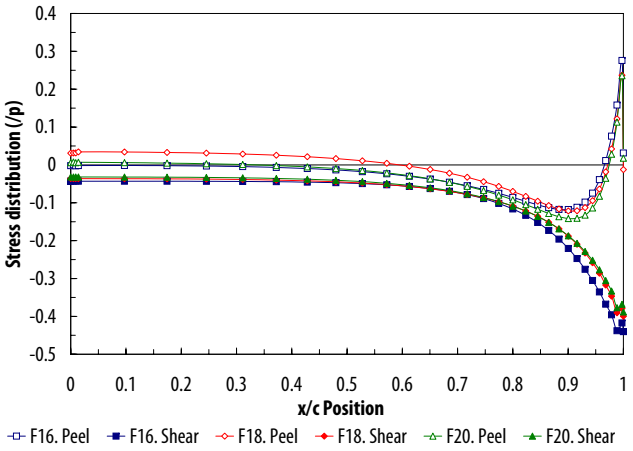

Fig. 16 Stress distribution in F16, F18 and F20 models, involving vertical discretization influence of the adherent mesh

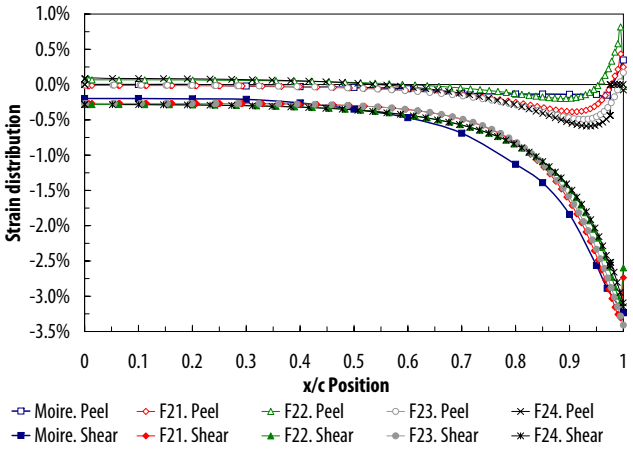

Fig. 17 Comparison of strains measured in Tsai and Morton's Moire experiment [6] and the F21, F22 and F23 models, involving element type influence

tion time advise against the use of an excessive number of these elements in the thickness of the adherends. It is also observed a logical correlation between the number of nodes and the time of analysis, except for the models F11 and F12, that present higher times of calculation considering their mesh size. The explanation for this situation is that sometimes the convergence of the nonlinear analysis is deteriorated, specially with coarser meshes.

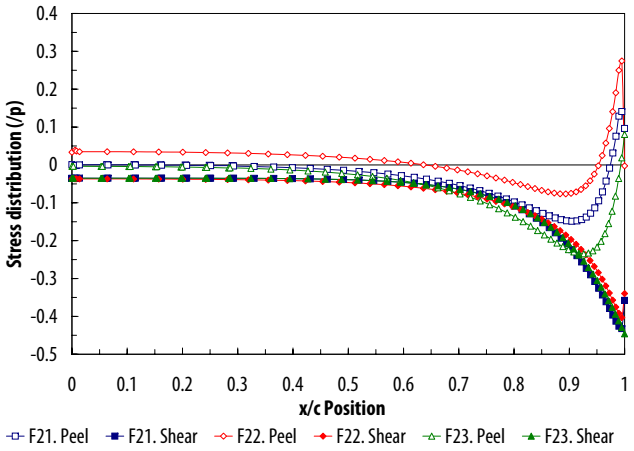

Fig. 18 Stress distribution in F21, F22 and F23 models, involving element type influence

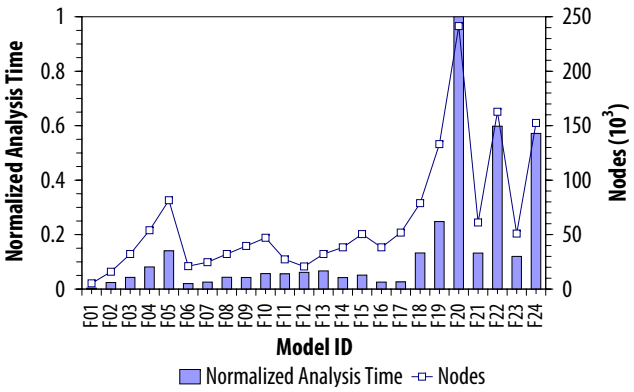

Fig. 19 Normalized analysis time and total number of nodes of each model

3.5 Adhesive Nonlinear Material Behaviour

Besides the geometrical nonlinearity already considered, it is important the consideration of material nonlinearities as much in the adherent as in the adhesive with the aim to reproduce the different collapse forms of the joint (delaminating in the adherend, peeling in the adhesive) and to calculate the ultimate load that the single lap could support.

In this new model we considered material nonlinearity only in the adhesive, keeping linear material in the adherend. The load applied in the previous examples has been linearly extended until the single lap reach collapse. The model used was F25 with 2200 elements, shell elements for the adherends and one layer of 3D cohesive elements in the adhesive (elements COH3D8 of

ABAQUS Finite Element Code [8] , [10]).

The Fig. 20 shows the nonlinear material law used in the analysis. We use a traction-separation linear damage law with an ultimate nominal stress (stress for damage beginning) value of $\sigma_u = 1500KPa$, uncoupled traction elastic behaviour in the initial branch with $E_{eff} = 3GPa$, initial separation failure for softening initiation $\delta_0 = 6.5 \cdot 10^{-5} m$, and failure separation of $\delta_f = 2 \cdot \delta_0$. With these parameters, the critical energy release rate G_c of the bond has the value of $G_c = 0.975KJ/m^2$.

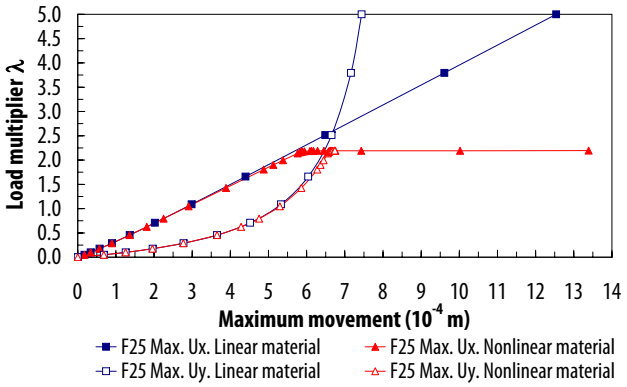

Fig. 20 Traction-separation damage model

The initiation failure criteria is applied to the adhesive normal traction stresses and to the two tractions related with the tangential stresses contained at the adhesive plane, whereas compression stresses are not limited.

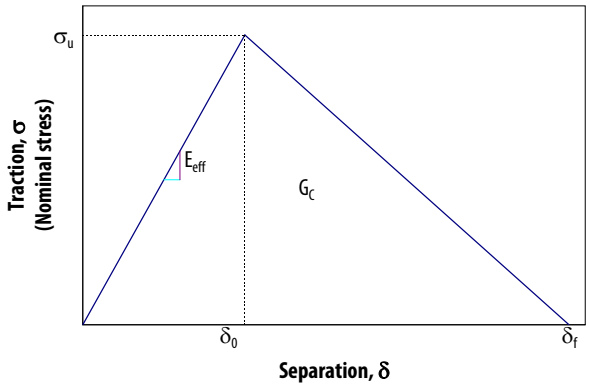

Fig. 21 Load versus maximum displacements for linear and nonlinear material models

Fig. 21 shows the global model response (Load level / displacements) for the linear material and the nonlinear material analysis. For the load level applied in the previous analysis (load multiplier $\lambda = 1$), longitudinal and transverse maximum displacements are slightly lower than if nonlinear cohesive material model were used. For $\lambda = 1$, damage only takes place at the longitudinal ends due to the higher stresses in these boundaries. When load is increased the damaged area is expanded toward the center and the degree of degradation in the border elements increases.

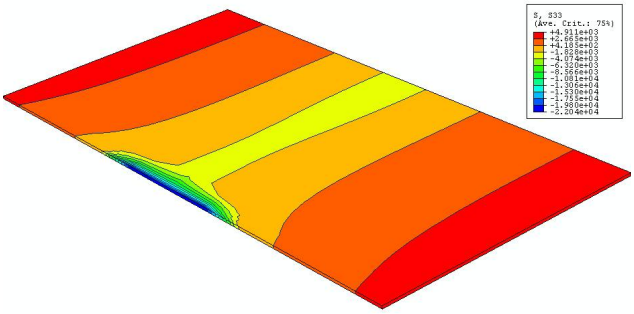

Fig. 22 Contour map of the σ_z peel stresses at the adhesive layer in the instant just before the collapse

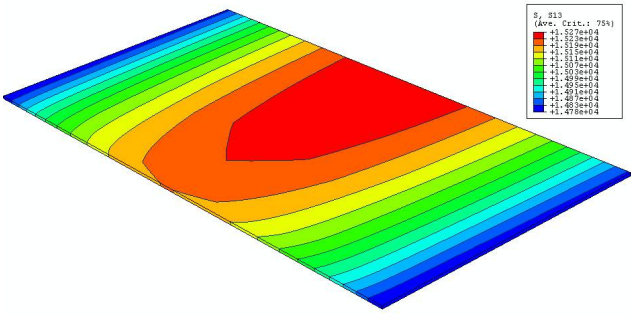

Fig. 23 Contour map of the τ_{xz} shear stresses at the adhesive layer in the instant just before the collapse

The joint breaking happens when the load is 2.19 times higher than the load applied in the previous section ($\lambda = 2.19$). Fig. 22 and Fig. 23 show normal and tangential stresses distribution in the adhesive for a step near to the collapse.

Future works could involve the development of the material nonlinearity approach in the

CFRP and in the adhesive, and to validate the obtained results by means of experimental research.

4 Conclusions

1. Modelling of three-dimensional meshes is feasible with the power of calculation of the present computers, allowing to introduce the joint in global models, something that the 2D models do not permit. On the other hand, the behavior outside the plane of the adherends of composite material is correlated in a more trustworthy way.

2. Is necessary to consider the geometrical nonlinearity of the joint, to avoid great errors in the stress and strain response. The computational cost does not increases excessively for considering this aspect.

3. The stress and strain concentrations results at the ends of the adhesive layer suggest us to refine the mesh in that zone, to be able to capture properly the extreme values, specially those of peeling, since the shear values do not present a very high gradient in that zone. Nevertheless, in the central zone a coarser mesh can be used, without affecting the quality of the results.

4. The use of shell elements in the adherents results in models with smaller computational cost without afecct to the exactitude of the results. That is the reason why in absence of other requirements, its use as opposed to solid elements is advisable.

5. The structural response in the middle line of the adhesive is not significantly affected by increasing the number of element layers, although it is necessary in the case that we want to obtain distributions of results throughout the thickness.

Acknowledgements

The authors gratefully acknowledge to the CESGA, Supercomputation Center of Galicia (Spain), the computational resources supplied.

References

[1] O. Volkersen. Die nietkraftverteilung in zugbeanspruchten nietverbindungen mit konstanten laschenquerschnitten. *Luftfahrtforschung*, 35:4–47, 1938.

[2] M. Goland and E. Reissner. The stresses in cemented joints. *Journal of Applied Mechanics*, 11:A17–27, 1944.

[3] L. J. Hart-Smith. Adhesive-bonded single-lap joints. Technical Report NASA CR 112236, National Aeronautics and Space Administration, 1973.

[4] L. J. Hart-Smith. Analysis and design of advanced composite bonded joints. Technical Report NASA CR 2218, National Aeronautics and Space Administration, 1974.

[5] M. Y. Tsai and J. Morton. Three-dimensional deformations in a single-lap joint. *Journal of Strain Analysis for Engineering Design*, 29(2):137, 1994.

[6] M. Y. Tsai and J. Morton. The effect of a spew fillet on adhesive stress distributions in laminated composite single-lap joints. *Composite Structures*, 32(1-4):123, 1995.

[7] Gang Li, Pearl Lee-Sullivan, and Ronald W. Thring. Nonlinear finite element analysis of stress and strain distributions across the adhesive thickness in composite single-lap joints. *Composite Structures*, 46(4):395 – 403, 1999.

[8] *ABAQUS 6.5.5. Standard User's Manual*. ABAQUS, Inc., Pawtucket, Rhode Island, 2005.

[9] Robert D. Cook, David S. Malkus, Michael E. Plesha, and Robert J. Witt. *Concepts and Applications of Finite Element Analysis*. John Wiley & Sons, New York, 4 edition, 2001.

[10] T. Diehl. Using abaqus cohesive elements to model peeling o fan epoxy-bonded aluminum strip: A benchmark study for inelastic peel arms. In *Abaqus Usert's Conference*, 2006.